JB
Journals.ASM.org

Wall Teichoic Acids Restrict Access of Bacteriophage Endolysin Ply118, Ply511, and PlyP40 Cell Wall Binding Domains to the *Listeria monocytogenes* Peptidoglycan

Marcel R. Eugster and Martin J. Loessner

Institute of Food, Nutrition and Health, ETH Zurich, Zurich, Switzerland

The C-terminal cell wall binding domains (CBDs) of phage endolysins direct the enzymes to their binding ligands on the bacterial cell wall with high affinity and specificity. The *Listeria monocytogenes* Ply118, Ply511, and PlyP40 endolysins feature related CBDs which recognize the directly cross-linked peptidoglycan backbone structure of *Listeria*. However, decoration with fluorescently labeled CBDs primarily occurs at the poles and septal regions of the rod-shaped cells. To elucidate the potential role of secondary cell wall-associated carbohydrates such as the abundant wall teichoic acid (WTA) on this phenomenon, we investigated CBD binding using *L. monocytogenes* serovar 1/2 and 4 cells deficient in WTA. Mutants were obtained by deletion of two redundant *tagO* homologues, whose products catalyze synthesis of the WTA linkage unit. While inactivation of either *tagO1* (EGDe *lmo0959*) or *tagO2* (EGDe *lmo2519*) alone did not affect WTA content, removal of both alleles following conditional complementation yielded WTA-deficient *Listeria* cells. Substitution of *tagO* from an isopropyl-β-D-thiogalactopyranoside-inducible single-copy integration vector restored the original phenotype. Although WTA-deficient cells are viable, they featured severe growth inhibition and an unusual coccoid morphology. In contrast to CBDs from other *Listeria* phage endolysins which directly utilize WTA as binding ligand, the data presented here show that WTAs are not required for attachment of CBD118, CBD511, and CBDP40. Instead, lack of the cell wall polymers enables unrestricted spatial access of CBDs to the cell wall surface, indicating that the abundant WTA can negatively regulate sidewall localization of the cell wall binding domains.

Bacteriophage endolysins are cell wall-hydrolyzing enzymes produced during the late phase of gene expression in the lytic cycle of virus multiplication, mediating the release of progeny phages (3, 32). They are usually composed of two functional domains, an enzymatically active domain (EAD) at the N terminus and a cell wall binding domain (CBD) at the C-terminal part of the protein. Although endolysins have attracted attention as prospective tools and antimicrobial agents (3, 17, 21, 32), surprisingly little is known about the identity and structure of their cell wall-associated CBD binding ligands.

The cell envelope of a typical Gram-positive organism is composed of peptidoglycan, proteins, and secondary cell wall polymers, including teichoic acids (TAs) and other glycopolymers. Peptidoglycan together with the attached polymer chains plays a crucial role in bacterial physiology and assumes a variety of other functions (28, 35, 54). TAs represent the most abundant polymer associated with the cell walls of Gram-positive bacteria and include cell wall-anchored wall teichoic acids (WTAs) and membrane-anchored lipoteichoic acids (LTAs), differing in synthesis and chemical structure (37). WTAs are phosphate-containing, anionic carbohydrate polymers covalently attached to the peptidoglycan via a conserved linkage unit (37, 52). Although their structures may be highly variable between species or even strains (54), the repeating units of the WTA polymers often feature glycerol phosphate (e.g., in *Bacillus subtilis* 168) or ribitol phosphate (e.g., in *Staphylococcus aureus* and *Listeria monocytogenes*) backbones (56) and are often modified and substituted with different sugars or amino acids, such as D-alanine (27, 37). LTAs usually show less structural diversity (54). In *L. monocytogenes*, LTA polymers consist of hydrophilic poly(glycerol phosphate) chains decorated with D-alanine and galactosyl residues (23, 39, 50).

The CBD of *Listeria* phage endolysin PlyP35 specifically recognizes *N*-acetylglucosamine (GlcNAc) residues attached to the ribitol phosphate in WTA polymers of *L. monocytogenes* serovar 1/2 and 3 strains (11). In contrast, the CBDs of *Listeria* phage endolysins Ply118, Ply511, and PlyP40 (34, 43) investigated here are assumed to recognize a more common, serovar-independent motif in the peptidoglycan structure (43). Green fluorescent protein (GFP)-tagged CBD118, CBD511, and CBDP40 molecules mainly attach to poles and septal regions of *Listeria* cells (33, 43), while the nature of the binding ligands remains unclear. The specific spatial distribution of binding ligands on the *Listeria* cell surface could also suggest that CBD targeting might be regulated and/or affected by the presence of other components in the cell envelope, such as the extremely abundant WTA polymers, which were reported to constitute up to 70% of the *Listeria* cell wall dry weight (13, 14).

Although WTA polymers are not essential for viability in *B. subtilis* and *S. aureus*, they contribute to host-cell binding, immune evasion, and virulence properties (8, 53, 54, 56). *B. subtilis* and *S. aureus* cells devoid of WTAs have been obtained by inactivation of *tagO*, whose product initiates the first step in WTA synthesis, transfer of GlcNAc phosphate to its lipid carrier, undecaprenyl phosphate (45, 53). The situation in *L. monocytogenes* had not been investigated, until now. Therefore, the aim of this study was to define the ligands in the bacterial cell envelope responsible

Received 8 May 2012 **Accepted** 18 September 2012
Published ahead of print 21 September 2012
Address correspondence to Martin J. Loessner, martin.loessner@ethz.ch.
Supplemental material for this article may be found at http://jb.asm.org/.

doi:10.1128/JB.00808-12

TABLE 1 Bacterial strains and plasmids[a]

Strain or plasmid	Relevant characteristics	Reference or origin
Listeria monocytogenes strains		
EGDe	Wild type; serovar 1/2a	J. Kreft
WSLC 1042	Wild type; serovar 4b	ATCC 23074
EGDeΔ*tagO1*	EGDeΔ*lmo0959*; EGDe carrying a chromosomal deletion of *lmo0959*	This study
EGDeΔ*tagO2*	EGDeΔ*lmo2519*; EGDe carrying a chromosomal deletion of *lmo2519*	This study
1042Δ*tagO1*	1042Δ*LMO1042_0979*; WSLC 1042 carrying a chromosomal deletion of *LMO1042_0979*	This study
1042Δ*tagO2*	1042Δ*LMO1042_2492*; WSLC 1042 carrying a chromosomal deletion of *LMO1042_2492*	This study
EGDeΔ*tagO1*Δ*tagO2*::pLIV2(*tagO1*)	EGDe with a double deletion (Δ*lmo0959* and Δ*lmo2519*) and *lmo0959* expressed from an IPTG-inducible promoter; Cam^r IPTG (+/−)[b]	This study
1042Δ*tagO1*Δ*tagO2*::pLIV2(*tagO1*)	WSLC 1042 with a double deletion (Δ*LMO1042_0979 and* Δ*LMO1042_2492*) and *LMO1042_0979* expressed from an IPTG-inducible promoter; Cam^r IPTG (+/−)	This study
Escherichia coli strains		
XL1-Blue MRF′	Used for plasmid manipulations; Δ(*mcrA*)*183* Δ(*mcrCB-hsdSMR-mrr*)*173 endA1 supE44 thi-1 recA1 gyrA96 relA1 lac* [F′ *proAB lacI*^{q}*Z*ΔM15 Tn*10* (Tet^r)]	Stratagene
XL1-Blue MRF′ pHGFP_CBD118	Used for protein expression of HGFP_CBD118; Amp^r Tet^r	33
XL1-Blue MRF′ pHGFP_CBD511	Used for protein expression of HGFP_CBD511; Amp^r Tet^r	43
XL1-Blue MRF′ pHGFP_CBDP40	Used for protein expression of HGFP_CBDP40; Amp^r Tet^r	43
XL1-Blue MRF′ pHGFP_CBDP35	Used for protein expression of HGFP_CBDP35; Amp^r Tet^r	43
Plasmids		
pKSV7	Gram-negative bacterium/Gram-positive bacterium shuttle vector; thermosensitive; 6.9 kb; Cam^r	44
pAUL-A	Gram-negative bacterium/Gram-positive bacterium shuttle vector; thermosensitive; 9.2 kb; Ery^r	5
pLIV2	*L. monocytogenes* site-specific phage integration vector; IPTG-controlled expression; 6.1 kb; Cam^r	24
pKSV7(Δ*lmo0959*)	pKSV7 with *lmo0959* flanking regions; Cam^r	This study
pKSV7(Δ*lmo2519*)	pKSV7 with *lmo2519* flanking regions; Cam^r	This study
pKSV7(Δ*LMO1042_0979*)	pKSV7 with *LMO1042_0979* flanking regions; Cam^r	This study
pKSV7(Δ*LMO1042_2492*)	pKSV7 with *LMO1042_2492* flanking regions; Cam^r	This study
pAUL-A(Δ*lmo0959*)	pAUL-A with *lmo0959* flanking regions; Ery^r	This study
pAUL-A(Δ*LMO1042_0979*)	pAUL-A with *LMO1042_0979* flanking regions; Ery^r	This study
pLIV2(Δ*lmo0959*)	pLIV2 with *lmo0959* under IPTG control; Cam^r	This study
pLIV2(Δ*lmo0979*)	pLIV2 with *LMO1042_0979* under IPTG control; Cam^r	This study

[a] Genes *lmo0959* and *LMO1042_0979* were designated *tagO1*; genes *lmo2519* and *LMO1042_2492* were named *tagO2*.
[b] IPTG (+/−), IPTG was added when required to regulate the expression of *tagO1* under the control of the inducible P_{spac} promoter.

for binding of CBD118, CBD511, and CBDP40 and to explain the uneven spatial distribution of CBD molecules on *Listeria* cell walls. Toward this goal, we identified the key genes involved in WTA synthesis, which allowed us to construct WTA-deficient mutants in order to assess CBD binding and the role of WTA in this process.

MATERIALS AND METHODS

Bacteria, plasmids, and growth conditions. The strains and plasmids used in this study are listed in Table 1. *Escherichia coli* strains were cultured aerobically at 37°C in Luria-Bertani (LB) medium with shaking and used for cloning, amplification of plasmids, and recombinant protein synthesis. *L. monocytogenes* strains were grown in brain heart infusion (BHI) medium or tryptose broth (TB) at 30°C with shaking. The following antibiotics were added to broth as selective agents when appropriate: ampicillin (100 μg/ml for *E. coli*), chloramphenicol (10 μg/ml for *E. coli* and *L. monocytogenes*), erythromycin (300 μg/ml for *E. coli*, 10 μg/ml for *L. monocytogenes*), and tetracycline (30 μg/ml for *E. coli*) (Sigma-Aldrich, Buchs SG, Switzerland). Media were supplemented with IPTG (isopropyl-β-D-thiogalactopyranoside; 240 μg/ml; Carl Roth GmbH, Karlsruhe, Germany) for IPTG-inducible gene expression, if applicable.

General DNA techniques. General molecular biology techniques were performed by using standard protocols (40). Restriction enzymes and T4 DNA ligase (Roche Diagnostics, Rotkreuz, Switzerland) were used according to the manufacturer's protocols. DNase, RNase, and proteinase K were purchased from Fermentas (Le Mont-sur-Lausanne, Switzerland). DNA fragments and PCR products used for cloning and construction of plasmids were created with Phusion high-fidelity DNA polymerase (Finnzymes, Espoo, Finland). PCR products and DNA restriction fragments were purified with a GenElute PCR cleanup kit (Sigma-Aldrich). Plasmids were purified using a GenElute plasmid miniprep kit (Sigma-Aldrich). Oligonucleotides (see Table S1 in the supplemental material) were designed using the sequence of *L. monocytogenes* serovar 1/2a strain EGDe (GenBank accession no. AL591824) and serovar 4b strain F2365 (GenBank accession no. AE017262) (20, 36). All PCR products, plasmids, and correct insertions into chromosomal DNA of *L. monocytogenes* strains were verified by DNA sequencing.

***In silico* analysis.** Identification and sequence alignment of putative *tagO* homologues and the corresponding amino acid sequences were performed for *L. monocytogenes* strains EGDe and F2365, *Listeria innocua* Clip 11262 (GenBank accession no. AL592022), *Listeria seeligeri* SLCC 3954 (serovar 1/2b; GenBank accession no. FN557490), and *Listeria welshimeri* SLCC 5334 (serovar 6b; GenBank accession no. AM263198). Sequences were compared to the respective proteins from *B. subtilis* 168 and *S. aureus* MN8 using the NCBI BLAST tool (www.ncbi.nlm.nih.gov) and the software CLC Main Workbench (Aarhus, Denmark).

Deletion of *tagO* alleles in *L. monocytogenes*. Plasmids for allelic exchange and generation of *L. monocytogenes* in-frame deletion mutants EGDeΔ*tagO1* (EGDeΔ*lmo0959*), EGDeΔ*tagO2* (EGDeΔ*lmo2519*), 1042Δ*tagO1* (1042Δ*LMO1042_0979*), and 1042Δ*tagO2* (1042Δ*LMO1042_2492*) (Table 1)

were constructed by splicing by overlap extension PCR (SOE-PCR) (25). Genes of *L. monocytogenes* serovar 4b strain WSLC 1042 were named according to the annotated genome sequences of *L. monocytogenes* serovar 4b strain F2365. The SOE-PCR primers listed in Table S1 in the supplemental material were designed to amplify upstream (primer pair A and B) and downstream (primer pair C and D) fragments of relevant genes by using EGDe or WSLC 1042 chromosomal DNA as the template. Fragments with in-frame deletions were then generated in an SOE-PCR using products AB and CD and the external primers A and D. The resulting products (AD) were digested with SacI and BamHI and ligated into the corresponding sites of the temperature-sensitive shuttle vector pKSV7 (44). The constructs were transformed into *E. coli* strain XL1-Blue MRF′, resulting in pKSV7(Δ*lmo2519*) and pKSV7(Δ*lmo0959*), used for strain EGDe, as well as pKSV7(Δ*LMO1042_2492*) and pKSV7(Δ*LMO1042_0979*), used for strain WSLC 1042.

Isolated plasmids were then electroporated into competent *L. monocytogenes* EGDe or WSLC 1042 using a previously published protocol (38). On the basis of the temperature-sensitive origin of replication of pKSV7, chromosomal integration was selected at 42°C (nonpermissive temperature) in the presence of antibiotics. After a series of passages and growth at the permissive temperature (30°C) in the absence of selective drugs, deletion of target genes was obtained via homologous recombination and allelic replacement (44). Colonies were screened for the loss of antibiotic resistance. Antibiotic-sensitive mutants EGDeΔ*tagO1* and EGDeΔ*tagO2*, as well as 1042Δ*tagO1* and 1042Δ*tagO2*, were confirmed by PCR and DNA sequencing to verify in-frame deletions.

Inducible expression of *tagO*. *L. monocytogenes tagO1* genes *lmo0959* (strain EGDe) and *LMO1042_0979* (strain WSLC 1042), including their native ribosome binding sites, were amplified from chromosomal DNA using the primer pairs listed in Table S1 in the supplemental material. PCR products were digested with BamHI and PstI and inserted into pLIV2 (24) immediately downstream of the IPTG-inducible P_{spac} promoter. pLIV2 is an integrative shuttle plasmid derived from pLIV1 (6) and the site-specific integration vector pPL2 (30). The constructs pLIV2(Δ*lmo0959*) and pLIV2(Δ*lmo0979*) were electroporated into *E. coli* strain XL1-Blue MRF′, and purified plasmids were used as described below.

Conditional Δ*tagO1* Δ*tagO2* double-deletion mutants. Our initial attempts to delete both *tagO* alleles sequentially failed, since mutant bacteria were apparently not viable. In an alternative approach, we constructed conditional mutants using pLIV2(Δ*lmo0959*) and pLIV2(Δ*lmo0979*), to enable regulated expression of *tagO* under the control of the inducible promoter P_{spac}. Vector pLIV2(Δ*lmo0959*) was introduced into EGDeΔ*tagO1*, followed by selection for plasmid integration on BHI plates supplemented with chloramphenicol, yielding strain EGDeΔ*tagO1*::pLIV2(Δ*lmo0959*). Similarly, plasmid pLIV2(Δ*lmo0979*) was used to generate strain 1042Δ*tagO1*::pLIV2(Δ*lmo0979*). In the next step, conditional Δ*tagO1* Δ*tagO2* double-deletion mutants were constructed by allelic replacement using the temperature-sensitive shuttle vector pAUL-A (5) containing an erythromycin resistance marker. SOE-PCR products of Δ*lmo0959* and Δ*LMO1042_0979* digested with SacI and BamHI were cloned into pAUL-A, yielding pAUL-A(Δ*lmo0959*) and pAUL-A(Δ*LMO1042_0979*). After transformation into *Listeria*, insertion mutants were generated according to the procedure described above. Excision of chromosomally integrated plasmids was performed by repeated growth at 30°C in the absence of erythromycin but in the presence of chloramphenicol and 1 mM IPTG to maintain the pLIV2 recombinant plasmid in order to support cell growth and viability. Expression of genes under IPTG-inducible promoter control allowed the stepwise elimination of wild-type alleles. The resulting conditional *tagO*-null mutants were designated EGDeΔ*tagO1*Δ*tagO2*::pLIV2(*tagO1*) and 1042Δ*tagO1*Δ*tagO2*::pLIV2(*tagO1*). All constructs were confirmed by PCR and sequence analysis.

Properties of *tagO*-deficient *Listeria*. To determine the role of *tagO* for survival and viability of *Listeria*, growth of conditional *tagO*-null mutants was monitored in BHI medium without IPTG and compared to wild-type and *tagO* single-allele-deletion mutants. Conditional double-deletion mutants were inoculated into BHI supplemented with chloramphenicol (10 μg/ml) and IPTG (1 mM) and cultured overnight at 30°C with shaking. Parent strains EGDe and WSLC 1042 and the Δ*tagO1* and Δ*tagO2* mutants were grown in BHI without supplements. Then, cells were harvested, washed with BHI to remove residual IPTG and chloramphenicol, and resuspended in fresh BHI medium at a dilution of 1:100. The optical density at 600 nm (OD_{600}) of each culture during growth at 30°C was then monitored.

Purification of *Listeria* cell walls. Preparation of *L. monocytogenes* cell walls for the analysis of the cell wall phosphate content was performed as described previously (12, 15, 51, 55). Wild-type and mutant strains were cultivated in TB medium supplemented with antibiotics and IPTG, as required. The Δ*tagO1* Δ*tagO2* double-deletion mutants were precultured in TB medium containing IPTG, centrifuged, washed with IPTG-free medium, and resuspended into fresh IPTG-free medium at an OD_{600} of 0.01. Exponentially growing cells (OD_{600}, 0.7) were heat killed at 100°C for 30 min, harvested by centrifugation (7,000 × *g*, 15 min, 4°C), and resuspended in SM buffer (50 mM Tris HCl, 100 mM NaCl, 8 mM $MgSO_4$, pH 7.5). Cells were broken by two passages through a One-Shot cell disrupter (Constant cell disruption system; Northants, United Kingdom) at a pressure of 270 MPa. Larger debris and remaining intact cells were removed by centrifugation at 1,500 × *g* for 5 min. Cell walls were recovered by centrifugation of the supernatant (20,000 × *g*, 30 min, 4°C). The cell wall-containing pellet was washed three times with water and resuspended in SM buffer. DNase/RNase (25°C, 4 h) and proteinase K (25°C, 2 h) were added at a concentration of 100 μg/g cell wall wet weight. Then, the same volume of 8% (wt/vol) boiling SDS was added, followed by further incubation for 30 min at 100°C to remove noncovalently associated components such as membranes, proteins, and LTAs. SDS-insoluble material was collected by centrifugation (20,000 × *g*, 30 min, 20°C). Finally, the cell wall-containing pellet was washed five times in pure water by repeated centrifugation and resuspension, lyophilized, and stored at −20°C.

Determination of cell wall-associated phosphate. To determine the relative amount of WTA in cell walls of wild-type and mutant strains, lyophilized purified cell walls (i.e., murein and covalently attached WTA) were assayed for total (cell wall-bound) phosphate as described elsewhere (12). Briefly, 0.1 mg purified peptidoglycan dissolved in 5 ml distilled water was treated with decomposition reagent (NANOCOLOR NanOx metal; Macherey-Nagel, Switzerland) for oxidative decomposition of cell walls according to the manufacturer's protocol. Subsequently, total phosphorus was determined using a photometric phosphate test (Spectroquant phosphate; Merck, Zug, Switzerland).

CBD binding and fluorescence microscopy. GFP-tagged CBD proteins derived from phage endolysins Ply118, Ply511, PlyP40, and PlyP35 were produced in *E. coli* and purified by affinity chromatography as described earlier (33, 43). Protein concentration was determined using a NanoDrop ND-1000 analyzer, and purity was checked by SDS-PAGE analysis. Binding of GFP-CBD to bacteria was tested as described before (33). Cells were grown overnight in BHI medium (30°C with shaking) supplemented with antibiotics and IPTG as indicated. Then, cultures were diluted 10-fold into fresh medium and incubated for another 2 h. In case of the conditional double-deletion mutants, overnight cultures were sedimented by centrifugation, washed once with prewarmed BHI, resuspended in fresh medium, and used to inoculate growth medium without IPTG. Bacterial samples (2 to 5 ml) were collected in the late log phase (centrifugation at 7,000 × *g* for 1 min), washed with phosphate-buffered saline–Tween 20 (PBS-T) buffer (50 mM NaH_2PO_4, 120 mM NaCl, 0.1% Tween 20, pH 8.0), and resuspended in 1/10 volume PBS-T. For binding assays, 100 μl of the resuspended cells was mixed with 50 μl of an 800 nM solution of the GFP-CBD proteins, and the mixture was incubated for 5 min at room temperature. Cells and bound protein were pelleted at 16,000 × *g* for 1 min, resuspended and washed twice in 500 μl PBS-T, and finally, resuspended in 50 μl PBS-T and analyzed by confocal laser scanning fluorescence microscopy (Leica TCS SPE; Leica, Heerbrugg, Switzerland) using GFP-specific excitation and emission wavelengths.

To permeabilize and remove the outer membrane of *E. coli* cells for

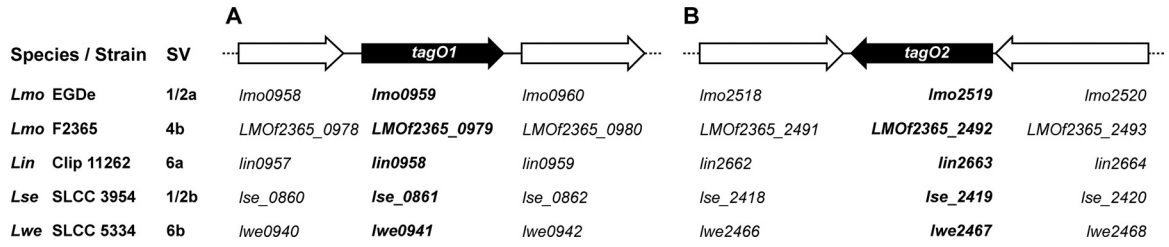

Species / Strain	SV						
Lmo EGDe	1/2a	*lmo0958*	***lmo0959***	*lmo0960*	*lmo2518*	***lmo2519***	*lmo2520*
Lmo F2365	4b	*LMOf2365_0978*	***LMOf2365_0979***	*LMOf2365_0980*	*LMOf2365_2491*	***LMOf2365_2492***	*LMOf2365_2493*
Lin Clip 11262	6a	*lin0957*	***lin0958***	*lin0959*	*lin2662*	***lin2663***	*lin2664*
Lse SLCC 3954	1/2b	*lse_0860*	***lse_0861***	*lse_0862*	*lse_2418*	***lse_2419***	*lse_2420*
Lwe SLCC 5334	6b	*lwe0940*	***lwe0941***	*lwe0942*	*lwe2466*	***lwe2467***	*lwe2468*

FIG 1 Genome regions harboring *tagO* homologues in the chromosomes of different *Listeria* strains. *tagO1* (A) and *tagO2* (B) genes from *Listeria* strains of different species and serovars (SV) are shown: *L. monocytogenes* (*Lmo*) EGDe (serovar 1/2a), *L. monocytogenes* strain F2365 (serovar 4b), *L. innocua* (*Lin*) Clip 11262 (serovar 6a), *L. seeligeri* (*Lse*) SLCC 3954 (serovar 1/2b), and *L. welshimeri* (*Lwe*) SLCC 5334 (serovar 6b). The *tagO* genes are shown as solid black arrows, and the individual gene designations are listed below. They are located at approximately opposite positions on the bacterial chromosomes.

determination of CBD decoration of the A1γ peptidoglycan of Gram-negative bacteria, cells were treated as described previously (31). Briefly, exponentially growing *E. coli* cells were centrifuged (7,000 × *g*, 5 min, 10°C), resuspended in chloroform-saturated 50 mM Tris buffer (pH 7.7), and incubated for 45 min at room temperature. Finally, cells were washed to remove the solvent, adjusted to an OD_{600} of 1.0, and used for the CBD binding assays described above.

RESULTS

Two homologous *tagO* genes in *L. monocytogenes*. The *tagO* products from *B. subtilis* and *S. aureus* have been shown to catalyze the first step in WTA biosynthesis, the transfer of GlcNAc to the bactoprenol carrier (45, 53). To provide a basis for the construction and analysis of WTA-deficient *Listeria* mutants, the first aim was to identify *tagO* homologues in the genomes of *L. monocytogenes* EGDe (serovar 1/2a) and F2365 (serovar 4b). Surprisingly, *in silico* analysis indicated two separate *tagO* orthologues with highly similar amino acid sequences (53% identity, 74% similarity) in the genomes of *L. monocytogenes* serovar 1/2 strain EGDe (genes *lmo0959* and *lmo2519*; GenBank accession numbers NP_464484 and NP_466042, respectively) and in *L. monocytogenes* serovar 4b strain F2365 (genes *LMOf2365_0979* and *LMOf2365_2492*; GenBank accession numbers YP_013580 and YP_015080, respectively) (Fig. 1). The genes are predicted to encode putative UDP-GlcNAc:undecaprenyl phosphate GlcNAc-1-phosphate transferases. Since they reveal significant homologies to the TagO proteins from *B. subtilis* and *S. aureus* (see Fig. S1 in the supplemental material; 42 to 49% amino acid identity and 66 to 71% similarity over the entire protein), we propose to use the *tagO* designation also for *Listeria*, although the specific transferase activities of these enzymes will have to be determined biochemically. Therefore, *lmo0959* and *LMOf2365_0979* are designated *tagO1*, while *lmo2519* (previously annotated *tagO* [2]) and *LMOf2365_2492* are named *tagO2*. In both cases, the apparently redundant *tagO* homologues are located at opposite positions on the bacterial genome and transcribed in different directions. At least *lmo2519* appears to be part of an operon structure (49). We have identified *tagO1* and *tagO2* homologues in all other available *Listeria* sp. genomes (*L. innocua* Clip 11262, *L. seeligeri* SLCC 3954, and *L. welshimeri* SLCC 5334) and found them to be highly similar (Fig. 1).

Deletion of *tagO* in *L. monocytogenes* serovar 1/2a and 4b strains. To determine the role of WTA polymers for recognition and binding of *Listeria* phage endolysins Ply118, Ply511, and PlyP40 (i.e., their CBDs), we constructed *tagO* deletion mutants in strains representing the two different WTA backbone types occurring in *L. monocytogenes* (18). Functional inactivation of *tagO* is expected to disrupt the first step of the WTA linkage unit biosynthetic pathway (45). We found that mutants featuring removal of a single allele (EGDeΔ*tagO1*, EGDeΔ*tagO2*, 1042Δ*tagO1*, and 1042Δ*tagO2*) showed absolutely no defects in growth or morphology. They were identical to the parent strains. This indicated that growth, division, and viability were not affected by removal of only one of the two apparently functionally redundant *tagO* alleles.

As a next step, we aimed to generate mutants defective in both genes, i.e., Δ*tagO1* Δ*tagO2* double deletions. However, all our attempts employing the classical two-step allelic replacement strategy were unsuccessful; i.e., the second exchange to inactivate the remaining *tagO* allele in EGDeΔ*tagO1*::pKSV7(Δ*tagO2*) and EGDeΔ*tagO2*::pKSV7(Δ*tagO1*) or in 1042Δ*tagO1*::pKSV7(Δ*tagO2*) and 1042Δ*tagO2*::pKSV7(Δ*tagO1*) failed. This finding suggested that at least one functional *tagO* locus is required and essential for normal cell growth and viability of *Listeria*. As a solution to the problem, we constructed double-deletion mutants which additionally feature conditional, regulated expression of *tagO1* from an integrated single-copy plasmid, which yielded strains EGDeΔ*tagO1*Δ*tagO2*::pLIV2(*tagO1*) and 1042Δ*tagO1*Δ*tagO2*::pLIV2(*tagO1*). Both mutants feature full in-frame chromosomal deletion of both *tagO* genes and a functional *tagO1* allele under the control of an IPTG-inducible promoter. Both strains were viable and used for further studies.

Deletion of *tagO* results in loss of WTA. To assess the impact of *tagO* deletion on WTA content in the *Listeria* peptidoglycan, the amount of phosphate (as a direct measure for WTA) present in purified cell walls of *tagO* single- and double-deletion mutants was determined and compared to that for the wild type. As shown in Fig. 2, deletion of only one of the two *tagO* alleles in strains EGDe and WSLC 1042 did not significantly affect the level of cell wall-associated phosphate in comparison to that for the wild type, confirming the functional redundancy of *tagO1* and *tagO2* in WTA biosynthesis. On the other hand, total phosphate associated with the cell walls of EGDeΔ*tagO1*Δ*tagO2*::pLIV2(*tagO1*) and 1042Δ*tagO1*Δ*tagO2*::pLIV2(*tagO1*) double-deletion mutants grown in the absence of IPTG was drastically reduced, to approximately 30 to 35% of the wild-type level. In the presence of IPTG, total cell wall phosphate in the conditional double-deletion mutants was almost completely restored to about 85 to 90% of that of the parental strain (33).

The *L. monocytogenes* serovar 1/2 EGDe mutant cells were also tested for decoration by fluorescent CBDP35, which specifically recognizes and binds to terminal GlcNAc residues attached to the

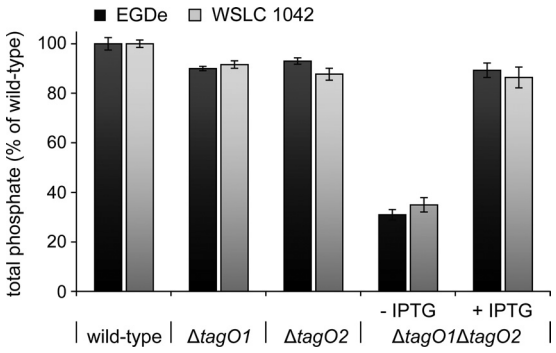

FIG 2 Cell wall teichoic acid depletion in *L. monocytogenes tagO* deletion mutants. Cell walls of serovar 1/2a (EGDe) and serovar 4b (WSLC 1042) wild-type strains, corresponding single-deletion mutants Δ*tagO1* and Δ*tagO2*, and conditional double-deletion mutants Δ*tagO1*Δ*tagO2*::pLIV2(*tagO1*) (abbreviated Δ*tagO1*Δ*tagO2*) grown in the presence or absence of IPTG (strains are listed in Table 1) were purified and analyzed for total cell wall-associated phosphorus as an indicator for the presence or absence of covalently linked cell wall teichoic acid. The diagram shows the effect of TagO deficiency on WTA content. Total phosphate is shown as relative values, whereupon the content in wild-type cell walls was defined as 100%. All measurements were carried out as independent triplicates.

poly(ribitol phosphate) backbone of *Listeria* WTA (11). Single *tagO1* or *tagO2* deficiency did not affect binding of CBDP35 (Table 2). In contrast, inactivation of both alleles in EGDeΔ*tagO1*Δ*tagO2*::pLIV2(*tagO1*) resulted in loss of decoration by CBDP35 (Table 2). These findings correlate well with those of the chemical analysis described above and provide additional evidence for the drastically reduced WTA level in these cells.

WTA deficiency leads to impaired growth and coccoid cell morphology. Single deletion of the *tagO* locus in EGDeΔ*tagO1*, EGDeΔ*tagO2*, 1042Δ*tagO1*, and 1042Δ*tagO2* did not affect cell morphology or growth properties compared to those of the wild type (Fig. 3). In contrast, inactivation of both alleles in EGDeΔ*tagO1*Δ*tagO2*::pLIV2(*tagO1*) and 1042Δ*tagO1*Δ*tagO2*::pLIV2(*tagO1*) was characterized by dramatic alterations in cell morphology (i.e., coccoid cells) and formation of aggregates when *tagO* expression was shut down following removal of IPTG. Additionally, WTA deficiency resulted in a substantially reduced growth rate, indicating a major role of WTA for normal cell growth and development. Transfer to IPTG-containing medium restored the normal phenotype (Fig. 2). These findings clearly indicate that the presence of at least one of the two redundant *tagO* homologues in *Listeria* is required for maintaining cell shape and growth response.

CBD118, CBD511, and CBDP40 do not require WTA for binding. To determine the potential role of the WTA polymers for binding of CBD118, CBD511, and CBDP40, *tagO* null mutants were tested for decoration by GFP-tagged CBDs (Table 2; Fig. 4). CBD511 and CBDP40 decorate the entire cell surface of wild-type EGDe and WSLC 1042, with a clear preference (i.e., more intensive decoration) for septal and polar regions (43). The same binding pattern was observed for mutant strains EGDeΔ*tagO1*, EGDeΔ*tagO2*, 1042Δ*tagO1*, and 1042Δ*tagO2*. Interestingly, binding of CBD511 and CBDP40 to the WTA-deficient double *tagO* null mutant was no longer restricted to poles and septa but occurred at a high density and was evenly distributed over the entire lateral (sidewall) cell surface.

Similar results were obtained for CBD118, which labeled the target cells at polar and septal regions (33). There was no difference in decoration of EGDe and the single-locus deletion mutants EGDeΔ*tagO1* and EGDeΔ*tagO2* (Table 2; Fig. 4). In contrast, CBD118 was found to decorate the entire cell surface of the WTA-deficient double-deletion mutant EGDeΔ*tagO1*Δ*tagO2*::pLIV2(*tagO1*). Binding to these cells appeared to be significantly stronger than that for the parental bacteria, as judged from fluorescence microscopy imaging. Moreover, WTA-deficient double-deletion mutants of serovar 4b strain WSLC 1042 were also found to be labeled by CBD118. This was a very surprising result, given the fact that CBD118 normally recognizes *Listeria* serovar 1/2 and 3 cells and does not bind to strains featuring serovar 4, 5, or 6 (33). Conditional double-deletion mutants grown in the presence of IPTG fully restored the wild-type CBD binding properties (Fig. 4).

The peptidoglycan of *Listeria* belongs to the *meso*-diaminopimelic acid (*m*-DAP) cross-linked A1γ chemotype, which is also featured by many Gram-negative bacteria, such as *E. coli* (42). In this context, the ability of CBD118, CBD511, and CBDP40 to decorate the peptidoglycan of *E. coli* cells stripped of their outer membrane (Fig. 5) further supports our conclusion that the different CBDs share the ability to recognize and bind to the A1γ peptidoglycan backbone.

Taken together, our findings demonstrate that CBD118, CBD511, and CBDP40 directly interact with the peptidoglycan

TABLE 2 Binding of GFP-tagged *Listeria* phage endolysin CBDs to *Listeria* cells

L. monocytogenes strain	Serovar	IPTG growth condition[a]	Presence of WTA[b]	Binding of CBD[c]			
				PlyP35	Ply511	Ply118	PlyP40
EGDe	1/2a		+	++	++	++	++
EGDeΔ*tagO1*			+	++	++	++	++
EGDeΔ*tagO2*			+	++	++	++	++
EGDeΔ*tagO1*Δ*tagO2*::pLIV2(*tagO1*)		+	+	++	++	++	++
EGDeΔ*tagO1*Δ*tagO2*::pLIV2(*tagO1*)		−	−	−	++	++	++
WSLC 1042	4b		+	−	+	−	++
1042Δ*tagO1*			+	−	+	−	++
1042Δ*tagO2*			+	−	+	−	++
1042Δ*tagO1*Δ*tagO2*::pLIV2(*tagO1*)		+	+	−	+	−	++
1042Δ*tagO1*Δ*tagO2*::pLIV2(*tagO1*)		−	−	−	++	++	++

[a] When required, IPTG was added to a final concentration of 1 mM.
[b] +, normal WTA content; −, reduced or no WTA content (determined by the amount of phosphate).
[c] ++, strong binding; +, weak binding; −, no binding (estimated by fluorescence microscopy, relative to wild-type EGDe or WSLC 1042).

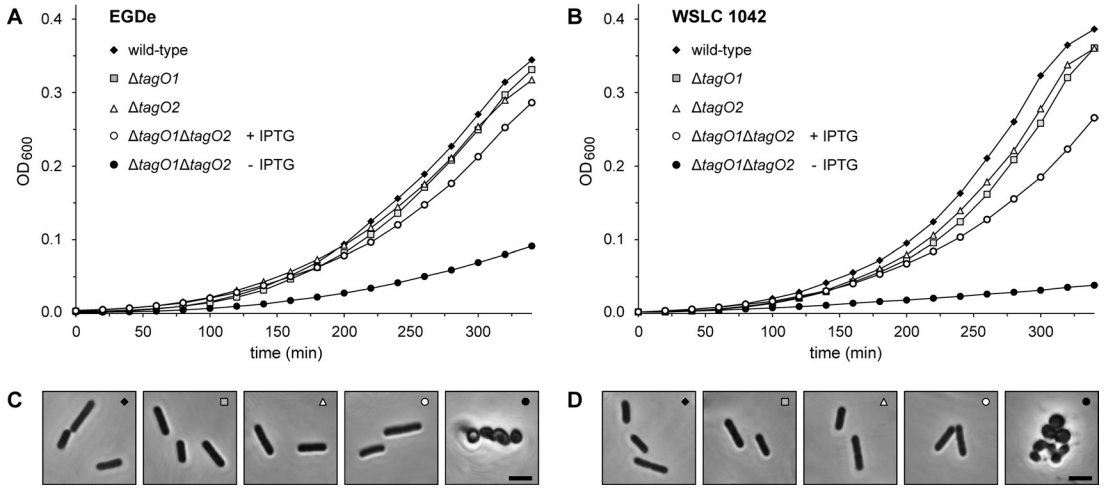

FIG 3 Effect of *tagO* disruption on growth and cell morphology of *L. monocytogenes*. Growth response and changes in cell morphology were analyzed for parental, single Δ*tagO1* and Δ*tagO2* deletions, and conditional Δ*tagO1* Δ*tagO2* double-deletion mutants. All cells were cultured in BHI broth without antibiotics, and conditional Δ*tagO1* Δ*tagO2* double-deletion mutants were grown in the presence or absence of IPTG. Growth was monitored (as OD_{600}) over the indicated time period. (A) *L. monocytogenes* serovar 1/2a wild-type strain EGDe and mutants EGDeΔ*tagO1*, EGDeΔ*tagO2*, and EGDeΔ*tagO1*Δ*tagO2*::pLIV2(*tagO1*) with and without IPTG. (B) *L. monocytogenes* serovar 4b wild-type strain WSLC 1042 and mutants 1042Δ*tagO1*, 1042Δ*tagO2*, and 1042Δ*tagO1*Δ*tagO2*::pLIV2(*tagO1*) with and without IPTG. (C and D) Phase-contrast microscopy of cell samples taken from log-phase cultures of strain EGDe and derivatives (C) and strain WSLC 1042 and derivatives (D). In the double-deletion mutants, the drastic effect of complete *tagO* functional disruption on cell shape and morphology is clearly visible. Bars, 2 μm.

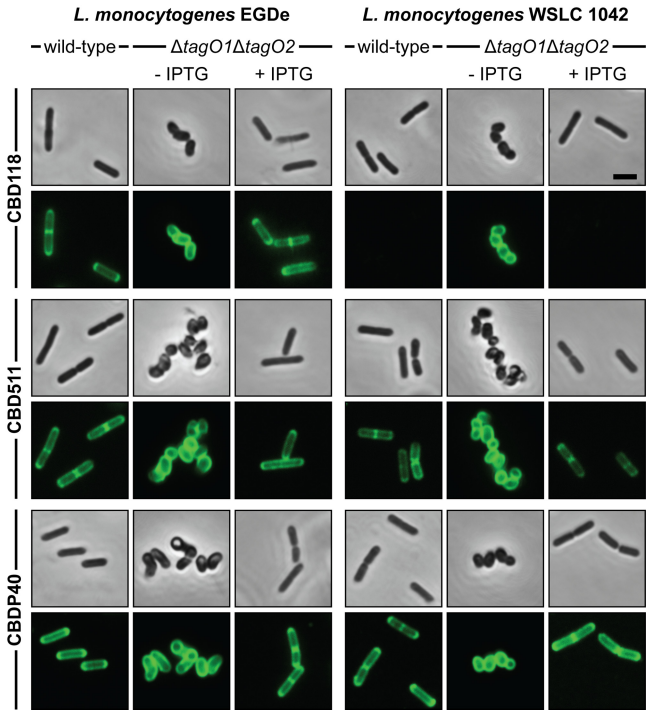

FIG 4 Targeting of CBD118, CBD511, and CBDP40 to *L. monocytogenes* cells and wall teichoic acid-deficient mutants. Wild-type *L. monocytogenes* EGDe (serovar 1/2a) and WSLC 1042 (serovar 4b) and corresponding conditional *tagO* double-deletion mutants EGDeΔ*tagO1*Δ*tagO2*::pLIV2(*tagO1*) and 1042Δ*tagO1*Δ*tagO2*::pLIV2(*tagO1*) (both indicated as Δ*tagO1*Δ*tagO2*) were exposed to different GFP-tagged *Listeria* phage CBD proteins (indicated on the left) (for details, see Materials and Methods). Conditional double-deletion mutants were grown in the presence or absence of IPTG. CBD binding was visualized by confocal laser scanning microscopy. The upper rows of each assay series show phase-contrast images of wild-type and mutant strains after CBD labeling, and the lower rows display the corresponding fluorescence images of the same field. Note the targeting of CBD118 to WTA-deficient *L. monocytogenes* WSLC 1042 cells. Bar, 2 μm.

backbone structure and that the WTA polymers present on *Listeria* cells are not required for this interaction. Moreover, their presence seems to negatively regulate access of the endolysin ligands for binding of the CBDs.

DISCUSSION

The mostly C-terminally located cell wall binding domains of endolysins from bacteriophages infecting Gram-positive bacterial host cells recognize specific peptidoglycan-associated ligands on the surface of the bacteria with high affinity and specificity. However, surprisingly few endolysin ligands have so far been identified. The Cpl-1 enzyme from pneumococcal phage Cp-1 and other pneumococcal endolysins use choline-binding modules for anchoring to choline-containing teichoic acids of the pneumococcal cell wall (19, 21, 22). Further, the C terminus of endolysin Lyb5, encoded by *Lactobacillus fermentum* bacteriophage ΦPYB5, has been shown to bind to the peptidoglycan, mediated by LysM

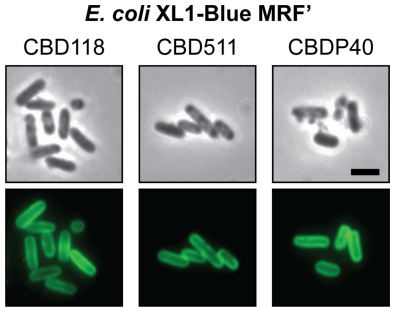

FIG 5 Binding of CBDs to *E. coli* peptidoglycan. Chloroform-treated *E. coli* XL1-Blue MRF′ cells were exposed to GFP-CBD118 (left), GFP-CBD511 (middle), and GFP-CBDP40 (right), to demonstrate the basic peptidoglycan-binding properties of the proteins. Samples were monitored by phase-contrast (upper row) and fluorescence (lower row) microscopy. Bar, 2 μm.

repeat regions (26). Regarding enzymes from *Listeria* phages, we recently reported that CBDP35 specifically recognizes terminal GlcNAc residues in the *Listeria* WTA molecules (11). In the work presented here, we show that the CBDs of *Listeria* phage endolysins Ply118, Ply511, and PlyP40 specifically interact with the peptidoglycan backbone structure of *Listeria* cells. In contrast to CBDP35, WTA polymers seem to be dispensable and are not required for recognition and binding. Instead, they apparently play a role in orchestrating the specific spatial localization of the endolysins to cell division sites and poles.

Use of GFP-tagged CBD fusion proteins to decorate cell walls of *Listeria* strains of different serovar types revealed individual binding partners of the different phage endolysins, which correlate very well with serovar- and strain-specific cell surface structures (33, 43). The binding patterns and properties of CBD118, CBD511, and CBDP40 differ fundamentally from those of other *Listeria* phage endolysin CBDs, such as CBD500, CBDPSA, and CBDP35 (29, 33, 43). The latter group of CBDs was found to recognize and bind to the entire cell surface, while CBD118, CBD511, and CBDP40 primarily associate with poles and septae (33, 43). Spatially distinct cell wall targeting has also been reported for other peptidoglycan hydrolases, such as *Lactobacillus* phage endolysin Lyb5 (26), the AcmA autolysin of *Lactococcus lactis* (46), and the Atl autolysin of *S. aureus* (41). The uneven distribution of these enzymes over the cell wall is also proposed to be due to the presence of secondary cell wall polymers such as teichoic acids that prevent targeting to the entire cell surface (41, 47).

Cell walls of *L. monocytogenes* contain two different polyanionic polymers: WTA, which is covalently linked to the peptidoglycan via a linkage unit, and LTA, which is anchored to the cytoplasmic membrane (35, 37). WTA polymers can account for up to 60 to 70% of the total dry mass of isolated *Listeria* cell walls (13, 14). During late log phase of bacterial growth, WTA polymers are evenly distributed over the entire cell surface. This is nicely illustrated by using fluorescent CBDP35 (11, 43), which targets the terminal GlcNAc substituted to position C-4 of the poly(ribitol phosphate) WTA backbone (11). In light of the findings described here, we postulate that the asymmetric distribution of CBD118, CBD511, and CBDP40 to the sites of cell division may also be based on WTA polymers. However, the polymers do not serve as binding ligands but seem to prevent an even distribution of the cell wall binding proteins to the peptidoglycan sacculus. The hypothesis was then tested and confirmed using WTA-deficient *Listeria* cells.

TagO catalyzes the initial step in synthesis of the WTA linkage unit, i.e., the formation of undecaprenyl-diphospho-*N*-acetylglucosamine (45, 48, 53). In order to gain better insight into WTA biosynthesis in *L. monocytogenes*, we made use of the fact that the WTA linkage units in Gram-positive bacteria feature conserved structures (1, 53). Based on sequence homologies with *B. subtilis* and *S. aureus* TagO, we identified two different *Listeria* genes designated *tagO1* and *tagO2*. As suggested earlier (56), the designation "*tag*" (teichoic acid glycerol) was used instead of "*tar*" (for teichoic acid ribitol), because of the highly conserved mechanisms in biosynthesis of the polymers. Our *in silico* and experimental analysis of *L. monocytogenes* TagO1 and TagO2 functions demonstrated their functional redundancy.

It was shown that *tagO* is not essential for cell viability in *B. subtilis* and *S. aureus* (8, 9), although mutants revealed growth and division defects. Along this line, deletion of *lmo2537* in *L. monocytogenes*, predicted to be involved in WTA linkage unit biosynthesis, resulted in a coccoid-like cell morphology (10) featuring a reduction in cell wall phosphate (48%) similar to that which we found for *L. monocytogenes tagO* double-deletion mutants. The low residual WTA level on these cells may be explained by leaky repression of *tagO1* transcription from the IPTG-dependent P_{spac} promoter on pLIV2 in the absence of the inducer. It might also originate from other phosphate-containing components (7) covalently attached to the bacterial cell wall, whereas LTA has been completely removed. The initial failure to generate and/or isolate *L. monocytogenes tagO* double-null mutants without conditional complementation was likely due to the severe growth deficiencies, which render isolation of the desired mutants from a pool of normally growing cells impossible. However, the possibility that simultaneous deletion of both *tagO* copies may be lethal for *Listeria* cannot be excluded.

Our findings demonstrate that WTA polymers do not directly serve as binding ligands for CBD118, CBD511, and CBDP40. Instead, in the absence of WTA, both the spatial distribution of these CBDs and the quality of binding differed fundamentally from those for wild-type strains; i.e., the CBDs were targeted to the entire cell surface with high intensity. This finding indicated that these CBDs recognize and bind to the peptidoglycan backbone structure itself and that their cell wall binding pattern is apparently dependent on an exclusion-based regulation mechanism by the abundant WTA molecules. This situation appears to be somewhat similar to what was reported for the division-associated autolysins Atl of *Staphylococcus aureus* (41) and AcmA in *L. lactis* (46). In the latter case, the even distribution of the autolysin is hindered by LTA. With respect to *Listeria* (16, 39), however, LTAs can safely be excluded as potential ligands for CBD binding. This is not only because their removal does not affect CBD targeting to isolated and purified cell walls (33) but also because they are structurally identical among the different species and serovars of *Listeria*, which does not correlate with the variable *Listeria* phage CBD binding patterns (33, 43).

Considering that the peptidoglycan backbone of *L. monocytogenes* is of the same chemotype featured by *E. coli* and many other Gram-negative bacteria (42), our data suggest that CBD118, CBD511, and CBDP40 recognize and bind type A1γ murein (directly cross-linked *m*-DAP). This would again correlate well with the broad, serovar-independent binding of CBD511 and CBDP40 (43). The fact that the different CBDs show strong binding to *E. coli* murein also excludes an enhancing effect of the morphological change of the coccoid-like *Listeria* on decoration by the CBDs. In conclusion, binding does not appear to be affected by cell shape but, rather, appears to be affected by the presence or absence of the secondary polymers.

However, several differences between the three CBD polypeptides exist. Ply118 and Ply511 share considerable homology in their CBDs (43% identity and 80% similarity) (34), which implies that they may be targeted to the same ligands in the peptidoglycan structure. However, these two CBDs do display somewhat different recognition properties. CBD118 can decorate *Bacillus megaterium* (33), which also features A1γ peptidoglycan (42), while CBD511 does not. CBDP40 targets several non-*Listeria* strains, including some members from the genera *Bacillus*, *Enterococcus*, *Staphylococcus*, and *Bifidobacterium* (43). Although identical or at least similar peptidoglycan structures may represent plausible reasons for the cross-reactions, CBD118, CBD511, and CBDP40 still

feature slightly different properties. These might be based on their similar but not identical amino acid sequences and on the existence of diverse and different peptidoglycan-binding motifs in the enzymes. CBDP40 has cell wall recognition motifs similar to bacterial SH3 and LysM motifs, whereas no such sequences could be identified in CBD118 and CBD511 (43). The peptidoglycan-binding properties of LysM domains appear to be dependent on other cell wall constituents, such as proteins, cell wall polymers, and even modifications of the peptidoglycan itself (4).

CBD118 offers the narrowest cell wall binding range, which correlates well with the host range of the parent A118 phage. This temperate phage infects *Listeria* serovar 1/2 strains only and does not recognize cells from serovars 4, 5, and 6 (33). Intriguingly, we show here that WTA-depleted serovar 4b cells (strain WSLC 1042) accept GFP-tagged CBD118 on the entire surface. This finding strongly suggests that the inability of CBD118 to target native serovar 4b cell walls is due to a mechanism of exclusion by the cell wall polymers.

In conclusion, the extremely abundant WTA polymers present on the *Listeria* cell surface assume crucial roles in the targeting and spatial distribution of phage endolysins CBD118, CBD511, and CBDP40 to septal and polar regions of the peptidoglycan. With increasing consideration of endolysins as potential antimicrobial agents and their cell wall binding domains as tools for immobilization and rapid detection of pathogens, molecular analysis of the endolysin and cell wall interactions becomes more and more important.

ACKNOWLEDGMENTS

We are grateful to Yves Briers (Catholic University of Leuven, Leuven, Belgium), Sibylle Schmitter (ETH Zurich, Zurich, Switzerland), and Vladimir Lazarevic (Université de Lausanne, Lausanne, Switzerland) for helpful discussions. Karin Hotz (ETH Zurich, Zurich, Switzerland) is acknowledged for critical reading of the manuscript.

REFERENCES

1. **Araki Y, Ito E.** 1989. Linkage units in cell walls of Gram-positive bacteria. Crit. Rev. Microbiol. **17**:121–135.
2. **Bierne H, Cossart P.** 2007. *Listeria monocytogenes* surface proteins: from genome predictions to function. Microbiol. Mol. Biol. Rev. **71**:377–397.
3. **Borysowski J, Weber-Dabrowska B, Gorski A.** 2006. Bacteriophage endolysins as a novel class of antibacterial agents. Exp. Biol. Med. (Maywood) **231**:366–377.
4. **Buist G, Steen A, Kok J, Kuipers OP.** 2008. LysM, a widely distributed protein motif for binding to (peptido)glycans. Mol. Microbiol. **68**:838–847.
5. **Chakraborty T, et al.** 1992. Coordinate regulation of virulence genes in *Listeria monocytogenes* requires the product of the *prfA* gene. J. Bacteriol. **174**:568–574.
6. **Dancz CE, Haraga A, Portnoy DA, Higgins DE.** 2002. Inducible control of virulence gene expression in *Listeria monocytogenes*: temporal requirement of listeriolysin O during intracellular infection. J. Bacteriol. **184**:5935–5945.
7. **D'Elia MA, Henderson JA, Beveridge TJ, Heinrichs DE, Brown ED.** 2009. The *N*-acetylmannosamine transferase catalyzes the first committed step of teichoic acid assembly in *Bacillus subtilis* and *Staphylococcus aureus*. J. Bacteriol. **191**:4030–4034.
8. **D'Elia MA, Millar KE, Beveridge TJ, Brown ED.** 2006. Wall teichoic acid polymers are dispensable for cell viability in *Bacillus subtilis*. J. Bacteriol. **188**:8313–8316.
9. **D'Elia MA, et al.** 2006. Lesions in teichoic acid biosynthesis in *Staphylococcus aureus* lead to a lethal gain of function in the otherwise dispensable pathway. J. Bacteriol. **188**:4183–4189.
10. **Dubail I, et al.** 2006. Identification of an essential gene of *Listeria monocytogenes* involved in teichoic acid biogenesis. J. Bacteriol. **188**:6580–6591.
11. **Eugster MR, Haug MC, Huwiler SG, Loessner MJ.** 2011. The cell wall binding domain of *Listeria* bacteriophage endolysin PlyP35 recognizes terminal GlcNAc residues in cell wall teichoic acid. Mol. Microbiol. **81**:1419–1432.
12. **Eugster MR, Loessner MJ.** 2011. Rapid analysis of *Listeria monocytogenes* cell wall teichoic acid carbohydrates by ESI-MS/MS. PLoS One **6**:e21500. doi:10.1371/journal.pone.0021500.
13. **Fiedler F.** 1988. Biochemistry of the cell surface of *Listeria* strains: a locating general view. Infection **16**(Suppl 2):92–97.
14. **Fiedler F, Ruhland GJ.** 1987. Structure of *Listeria monocytogenes* cell walls. Bull. Inst. Pasteur **85**:287–300.
15. **Fiedler F, Seger J, Schrettenbrunner A, Seeliger HPR.** 1984. The biochemistry of murein and cell-wall teichoic-acids in the genus *Listeria*. Syst. Appl. Microbiol. **5**:360–376.
16. **Fischer W, Mannsfeld T, Hagen G.** 1990. On the basic structure of poly(glycerophosphate) lipoteichoic acids. Biochem. Cell Biol. **68**:33–43.
17. **Fischetti VA.** 2005. Bacteriophage lytic enzymes: novel anti-infectives. Trends Microbiol. **13**:491–496.
18. **Fujii H, et al.** 1985. Structural study on teichoic acids of *Listeria monocytogenes* types 4a and 4d. J. Biochem. **97**:883–891.
19. **Garcia E, et al.** 1988. Molecular evolution of lytic enzymes of *Streptococcus pneumoniae* and its bacteriophages. Proc. Natl. Acad. Sci. U. S. A. **85**:914–918.
20. **Glaser P, et al.** 2001. Comparative genomics of *Listeria* species. Science **294**:849–852.
21. **Hermoso JA, Garcia JL, Garcia P.** 2007. Taking aim on bacterial pathogens: from phage therapy to enzybiotics. Curr. Opin. Microbiol. **10**:461–472.
22. **Hermoso JA, et al.** 2003. Structural basis for selective recognition of pneumococcal cell wall by modular endolysin from phage Cp-1. Structure **11**:1239–1249.
23. **Hether NW, Jackson LL.** 1983. Lipoteichoic acid from *Listeria monocytogenes*. J. Bacteriol. **156**:809–817.
24. **Higgins DE, Buchrieser C, Freitag NE.** 2006. Genetic tools for use with *Listeria monocytogenes*, p 620–633. *In* Fischetti VA, Novick RP, Ferretti JJ, Portnoy DA, Rood JI (ed), Gram-positive pathogens. American Society for Microbiology, Washington, DC.
25. **Horton RM, Hunt HD, Ho SN, Pullen JK, Pease LR.** 1989. Engineering hybrid genes without the use of restriction enzymes: gene splicing by overlap extension. Gene **77**:61–68.
26. **Hu S, Kong J, Kong W, Guo T, Ji M.** 2010. Characterization of a novel LysM domain from *Lactobacillus fermentum* bacteriophage endolysin and its use as an anchor to display heterologous proteins on the surfaces of lactic acid bacteria. Appl. Environ. Microbiol. **76**:2410–2418.
27. **Kohler T, Weidenmaier C, Peschel A.** 2009. Wall teichoic acid protects *Staphylococcus aureus* against antimicrobial fatty acids from human skin. J. Bacteriol. **191**:4482–4484.
28. **Kohler T, et al.** 2010. Teichoic acids, lipoteichoic acids and related cell wall glycopolymers of Gram-positive bacteria, p 75–91. *In* Microbial glycobiology. Academic Press, San Diego, CA.
29. **Korndörfer IP, et al.** 2006. The crystal structure of the bacteriophage PSA endolysin reveals a unique fold responsible for specific recognition of *Listeria* cell walls. J. Mol. Biol. **364**:678–689.
30. **Lauer P, Chow MY, Loessner MJ, Portnoy DA, Calendar R.** 2002. Construction, characterization, and use of two *Listeria monocytogenes* site-specific phage integration vectors. J. Bacteriol. **184**:4177–4186.
31. **Lavigne R, Briers Y, Hertveldt K, Robben J, Volckaert G.** 2004. Identification and characterization of a highly thermostable bacteriophage lysozyme. Cell. Mol. Life Sci. **61**:2753–2759.
32. **Loessner MJ.** 2005. Bacteriophage endolysins—current state of research and applications. Curr. Opin. Microbiol. **8**:480–487.
33. **Loessner MJ, Kramer K, Ebel F, Scherer S.** 2002. C-terminal domains of *Listeria monocytogenes* bacteriophage murein hydrolases determine specific recognition and high-affinity binding to bacterial cell wall carbohydrates. Mol. Microbiol. **44**:335–349.
34. **Loessner MJ, Wendlinger G, Scherer S.** 1995. Heterogeneous endolysins in *Listeria monocytogenes* bacteriophages: a new class of enzymes and evidence for conserved holin genes within the siphoviral lysis cassettes. Mol. Microbiol. **16**:1231–1241.
35. **Navarre WW, Schneewind O.** 1999. Surface proteins of Gram-positive bacteria and mechanisms of their targeting to the cell wall envelope. Microbiol. Mol. Biol. Rev. **63**:174–229.
36. **Nelson KE, et al.** 2004. Whole genome comparisons of serotype 4b and

1/2a strains of the food-borne pathogen *Listeria monocytogenes* reveal new insights into the core genome components of this species. Nucleic Acids Res. **32**:2386–2395.
37. **Neuhaus FC, Baddiley J.** 2003. A continuum of anionic charge: structures and functions of D-alanyl-teichoic acids in Gram-positive bacteria. Microbiol. Mol. Biol. Rev. **67**:686–723.
38. **Park SF, Stewart GS.** 1990. High-efficiency transformation of *Listeria monocytogenes* by electroporation of penicillin-treated cells. Gene **94**:129–132.
39. **Ruhland GJ, Fiedler F.** 1987. Occurrence and biochemistry of lipoteichoic acids in the genus *Listeria*. Syst. Appl. Microbiol. **9**:40–46.
40. **Sambrook J, Russell DW.** 2001. Molecular cloning: a laboratory manual, 3rd ed. Cold Spring Harbor Laboratory Press, Cold Spring Harbor, NY.
41. **Schlag M, et al.** 2010. Role of staphylococcal wall teichoic acid in targeting the major autolysin Atl. Mol. Microbiol. **75**:864–873.
42. **Schleifer KH, Kandler O.** 1972. Peptidoglycan types of bacterial cell walls and their taxonomic implications. Bacteriol. Rev. **36**:407–477.
43. **Schmelcher M, et al.** 2010. Rapid multiplex detection and differentiation of *Listeria* cells using fluorescent phage endolysin cell wall binding domains. Appl. Environ. Microbiol. **76**:5745–5756.
44. **Smith K, Youngman P.** 1992. Use of a new integrational vector to investigate compartment-specific expression of the *Bacillus subtilis spoIIM* gene. Biochimie **74**:705–711.
45. **Soldo B, Lazarevic V, Karamata D.** 2002. *tagO* is involved in the synthesis of all anionic cell-wall polymers in *Bacillus subtilis* 168. Microbiology **148**:2079–2087.
46. **Steen A, et al.** 2003. Cell wall attachment of a widely distributed peptidoglycan binding domain is hindered by cell wall constituents. J. Biol. Chem. **278**:23874–23881.
47. **Steen A, et al.** 2005. Autolysis of *Lactococcus lactis* is increased upon D-alanine depletion of peptidoglycan and lipoteichoic acids. J. Bacteriol. **187**:114–124.
48. **Swoboda JG, Campbell J, Meredith TC, Walker S.** 2010. Wall teichoic acid function, biosynthesis, and inhibition. Chembiochem **11**:35–45.
49. **Toledo-Arana A, et al.** 2009. The *Listeria* transcriptional landscape from saprophytism to virulence. Nature **459**:950–956.
50. **Uchikawa K, Sekikawa I, Azuma I.** 1986. Structural studies on lipoteichoic acids from four *Listeria* strains. J. Bacteriol. **168**:115–122.
51. **Valyasevi R, Sandine WE, Geller BL.** 1990. The bacteriophage kh receptor of *Lactococcus lactis* subsp. *cremoris* KH is the rhamnose of the extracellular wall polysaccharide. Appl. Environ. Microbiol. **56**:1882–1889.
52. **Ward JB.** 1981. Teichoic and teichuronic acids: biosynthesis, assembly, and location. Microbiol. Rev. **45**:211–243.
53. **Weidenmaier C, et al.** 2004. Role of teichoic acids in *Staphylococcus aureus* nasal colonization, a major risk factor in nosocomial infections. Nat. Med. **10**:243–245.
54. **Weidenmaier C, Peschel A.** 2008. Teichoic acids and related cell-wall glycopolymers in Gram-positive physiology and host interactions. Nat. Rev. Microbiol. **6**:276–287.
55. **Wendlinger G, Loessner MJ, Scherer S.** 1996. Bacteriophage receptors on *Listeria monocytogenes* cells are the *N*-acetylglucosamine and rhamnose substituents of teichoic acids or the peptidoglycan itself. Microbiology **142**:985–992.
56. **Xia G, Peschel A.** 2008. Toward the pathway of *S. aureus* WTA biosynthesis. Chem. Biol. **15**:95–96.